Conclusion

The existence of two distinct phases in the BaO–Al_2O_3 system with compositions intermediate between $BaAl_2O_4$ and Al_2O_3 has been clearly demonstrated. The more alumina-rich phase appears to be well-ordered and has a unit cell compatible with the MP or β type of structure, and symmetry $P6_3/mmc$. The second (Ba-rich) phase is found to be completely disordered, but there is clear evidence for a $\sqrt{3}a \times \sqrt{3}a$ supercell ordering in alternate mirror planes perpendicular to the c axis, with, however, imperfect ordering of the slabs along the c axis. Evidence for ordering in β''-aluminas has been found before (Boilet, Colin, Colomban & Comes, 1980), and Hansen & Bovin (1982) have found that a natural plumboferrite (nominal composition $PbFe_4O_7$) has diffraction patterns and images similar to those recorded here for phase II. Since this work was completed, Morgan & Shaw (1983) and Iyi, Takekawa, Bando & Kimura (1983) have also presented new evidence for the existence of two distinct phases in the $BaAl_2O_4$–Al_2O_3 system.

The ready intergrowth of the two phases suggests that conventional methods of phase and structure analysis in these and related systems may fail and that further electron optical studies are called for in other systems. These are in progress.

We are grateful to Drs J. C. H. Spence and J. Lynch, who first observed phases I and II by electron microscopy, for calling our attention to this problem, and to T. R. Wagner for some of the preparations. This work was supported by ARO contract DAAG29-80-C-0080 and by grant DMR-8119061 from the National Science Foundation and made use of the NSF HREM facility at Arizona State University.

References

ADELSKÖLD, V. (1938). *Ark. Kemi, Mineral. Geol.* **12A**, 1–9.
BOILET, J. P., COLIN, G., COLOMBAN, P. & COMES, R. (1980). *Phys. Rev. B*, **22**, 5912–5923.
BOVIN, J. O. & O'KEEFFE, M. (1980). *J. Solid State Chem.* **33**, 37–41.
BUXTON, B. E., EADES, J. A., STEEDS, J. W. & RACKHAM, G. M. (1976). *Philos. Trans. R. Soc. London Ser. A*, **281**, 171–194.
CLIFF, G. & LORIMER, G. W. (1976). *Proceedings of the 5th European Congress on Electron Microscopy*, p. 140. Bristol: Institute of Physics.
DUNN, B. & FARRINGTON, G. C. (1980). *Mater. Res. Bull.* **15**, 1773–1777.
HABEREY, F., OEHLSCHLEGEL, G. & SAHL, F. (1977). *Ber. Dtsch. Keram. Ges.* **54**, 373–378.
HANSEN, S. & BOVIN, J.-O. (1982). *Electron Microscopy* 1982, Vol. 2, pp. 27–28. Frankfurt: Deutsche Gesellschaft für Elektronenmikroskopie.
IYI, N., TAKEKAWA, S., BANDO, Y. & KIMURA, S. (1983). *J. Solid State Chem.* **47**, 34–40.
KIMURA, S., BANNAI, E. & SHINDO, I. (1982). *Mater. Res. Bull.* **17**, 209–215.
MORGAN, P. E. D. & CIRLIN, E. H. (1982). *J. Am. Ceram. Soc.* **65**, C114–C115.
MORGAN, P. E. D. & SHAW, J. M. (1983). *Mater. Res. Bull.* **18**, 539–542.
SPENCE, J. C. H. & LYNCH, J. (1982). *Ultramicroscopy*, **9**, 267–276.
STEVELS, A. L. N. (1978). *J. Lumin.* **17**, 121–133.
TORKAR, K., KRISCHNER, H. & MOSER, H. (1965). *Monatsh. Chem.* **96**, 423–429.
VERSTEGEN, J. M. P. J. (1973). *J. Solid State Chem.* **7**, 468–473.
VERSTEGEN, J. M. P. J. & STEVELS, A. L. N. (1974). *J. Lumin.* **9**, 406–414.

Acta Cryst. (1984). B**40**, 26–38

The Structure of $[Er(1)_{1-x}, Sn(1)_x]Er(2)_4Rh_6Sn(2)_4Sn(3)_{12}Sn(4)_2$, a Ternary Reentrant Superconductor

BY J. L. HODEAU AND M. MAREZIO

Laboratoire de Cristallographie, CNRS, Associé à l'USMG, BP 166*X*, 38042 *Grenoble, France*

AND J. P. REMEIKA

Bell Laboratories, Murray Hill, New Jersey 07974, *USA*

(*Received* 17 *January* 1983; *accepted* 2 *August* 1983)

Abstract

The structure of phase II in the Er–Rh–Sn system has been solved and refined from single-crystal X-ray diffraction data. It is described in the tetragonal system, space group $I4_1/acd$, with eight formulae per unit cell of dimensions $a = 13{\cdot}73$ and $c = 27{\cdot}42$ Å. The chemical formula is $[Er(1)_{1-x}Sn(1)_x]Er(2)_4Rh_6Sn(2)_4Sn(3)_{12}Sn(4)_2$, where Rh and Sn(3) correspond to two and four different crystallographic sites, respectively. All crystals are twinned by reticular pseudomerohedry. The atoms occupy the following positions: $M(1) \equiv [Er(1)_{1-x}Sn(1)_x]$ in $8(b)(00\frac{1}{4})$; $Rh_{[1]}$ in $16(d)(00z)$;

0108-7681/84/010026-13$01.50

$Sn(3)_{[1]}$ and $Sn(3)_{[2]}$ each in $16(f)(xx\frac{1}{4})$; Sn(4) in $16(e)(\frac{1}{4}x\frac{1}{8})$; and all the others in $32(g)(xyz)$. The refinement based on 954 independent reflections gave 0·033 and 0·031 as R and wR factors. Long-exposure precession photographs revealed the existence of weak reflections which, if taken into account, indicate that the space symmetry of phase II is lower than $I4_1/acd$. However, these extra reflections are about five to ten times weaker than the diffuse streaks observed in phase III. The 128 Sn(2) and Sn(3) atoms form a three-dimensional array of trigonal prisms whose centers are occupied by Rh atoms. This array consists of corner-sharing prism layers intercalated with isolated-prism layers along the [100], [010], and [001] directions. The large holes generated by this prism framework are occupied by $M(1)$ and Er(2) atoms. The weak diffuse streaks are due to partial ordering between Er(1) and Sn(1) over the $M(1)$ sites. These atoms are surrounded by 12 Sn(3) atoms forming a slightly distorted cuboctahedron while Er(2) atoms occupy sites enclosed by 10 Sn atoms, 9 of which belong to the prism framework and form a truncated cuboctahedron. The tenth atom is an Sn(4) which takes the place of the three missing atoms of the cuboctahedron. A detailed analysis of the interatomic distances and coordination numbers indicates that $M(1)$, Er(2), and Rh atoms have a cation-like behavior whereas Sn(2) and Sn(3) are anion-like. Sn(4) atoms participate as anions to the coordination polyhedra of the Er(2) atoms, but do not take part in the formation of the prism network. They are bonded to two Er(2) and two Sn(3) atoms. This cluster of three Sn atoms is a unique feature of the phase II structure. The description in terms of coordination polyhedra built up of cation-like and anion-like atoms is not complete as the structure contains strong metallic bonds among atoms forming isolated clusters.

Introduction

Four different phases have been characterized in the M–Rh–Sn system, M being La–Lu, Y, Sc, Ca, Sr, and Th (Remeika *et al.*, 1980; Cooper, 1980; Espinosa, 1980; Hodeau, Marezio, Remeika & Chen, 1982). Phases I and I′ correspond to the chemical formula: $Sn(1)M_3Rh_4Sn(2)_{12}$. Phase I exists when M = Eu, Yb, Ca, Sr, or Th, and phase I′ is found when M = La, Ce, Pr, Nd, Sm, or Gd, respectively. The structure of phase I is cubic, space group $Pm3n$, with a lattice parameter of about 9·7 Å (Vandenberg, 1980; Hodeau, Chenavas, Marezio & Remeika, 1980), while that of phase I′ is a superstructure of phase I. Its symmetry is still unknown since the superstructure spots can be indexed either on a body-centered cubic cell with $a_I' = 2a_I$ or on a triple-twinned tetragonal one with $a_I/\sqrt{2}c_I' = c_I$ (Hodeau *et al.*, 1982). The structural arrangement of these two phases consists of a three-dimensional network of corner-sharing Sn(2) trigonal prisms whose centers are occupied by Rh atoms. The Sn(1) and M atoms occupy 12-coordinated holes and form a sublattice which has exactly the same arrangement as that found in the structure of $A15$ compounds. The main effect of the distortion observed in phase I′ should be the lowering of site symmetry which would favor disorder between Sn(1) and M atoms.

Phase II, which exists for M = Ho–Lu, or with Y or Sc, is tetragonal with cell dimensions $a_{II} \sim 13{\cdot}75$ and $c_{II} \sim 27{\cdot}4$ Å. Its structure is closely related to that of phase III which exists for M = Tb–Tm. From powder and classical single-crystal X-ray diffraction data phase III appeared to be cubic, $a_{III} \simeq 13{\cdot}75$ Å and space group $F\bar{4}3m$. However, electron diffraction and long-exposure precession photographs revealed intermittent diffuse streaks exactly where the spots responsible for doubling the c axis appeared in phase II. This indicated that the tetragonality of phase II existed also in phase III, but only in short-range fashion (Chenavas, Hodeau, Collomb, Marezio, Remeika & Vandenberg, 1980).

Since these compounds have remarkable superconducting and magnetic properties (Remeika *et al.*, 1980; Lambert *et al.*, 1980; Ott, Odoni, Fisk & Remeika, 1980) we have undertaken a continuing program for their characterization. We report herein the crystal structure of phase II for the Er compound, which exhibits reentrant superconductivity ($T_c = 0{\cdot}97$ and $T_M = 0{\cdot}57$ K).

Twinning and space group

A Guinier powder pattern of phase II for the Er–Rh–Sn compound, taken with Fe $K\alpha$ radiation, was indexed on a tetragonal cell of dimensions $a_{II} = b_{II} = 13{\cdot}733\,(1)$ and $c_{II} = 27{\cdot}418\,(3)$ Å. However, lattice parameters corresponding to differently prepared batches differed among them by more than seven times the standard deviations, so that values such as 13·73 (1) and 27·42 (2) Å are more realistic.

Precession photographs taken with Mo $K\alpha$ radiation are readily indexed with the same tetragonal cell; nevertheless, superstructure reflections which are responsible for the doubling of the c axis appear along each of the three pseudocubic ⟨100⟩ directions. Fig. 1 shows a precession photograph corresponding to the $(2kl)_c$ plane of the pseudocubic $2a_{II} \times 2a_{II} \times c_{II}$ lattice. It can be seen that the doubling occurs along the $[010]_c$ and $[001]_c$ directions. The same feature is obtained with the $(h2l)_c$ and $(hk2)_c$ planes where the doubling occurs along the $[100]_c$,$[001]_c$ and $[100]_c$,$[010]_c$ directions, respectively.

As the difference between $2a_{II}$ and c_{II} is very small (for instance for the Er–Rh–Sn compound it is 0·048 Å), twin formation has to be expected in the tetragonal phases. From the intensity distribution of the superstructure spots and the displacement from

the tetragonal lattice modes of some of them, it can be deduced that the triple doubling is due to twinning by the pseudothreefold axes $[111]_c$, $[\bar{1}11]_c$, $[1\bar{1}1]_c$, $[\bar{1}\bar{1}1]_c$ of the pseudocubic $2a_{II} \times 2a_{II} \times c_{II}$ lattice. Figs. 1 and 2 show precession photographs and their schematic representation, the precession axes being $[100]_c$ and $[111]_c$ respectively. The tetragonal c/a ratio of 1·9965 corresponds to an angle of 0·05° between the pseudothreefold axis $[11\frac{1}{2}]_T$ of the $a_{II} \times a_{II} \times c_{II}$ cell and the threefold [111] axis of the cubic $a_{II} \times a_{II} \times a_{II}$ lattice. Since the unit-cell volume of the twinned crystals ($8a^3$) is a multiple of that of the single crystal ($2a^3$), twinning is by reticular pseudomerohedry.

For each $(hkl)_T$ reflection of the tetragonal structure the pseudothreefold axis $[11\frac{1}{2}]_T$ generates two other reflections such as $(l/2,h,2k)_T$ and $(k,l/2,2h)_T$. Because of the existence of the fourfold axis the operations of the other three pseudothreefold axes $[\bar{1}1\frac{1}{2}]_T$, $[1\bar{1}\frac{1}{2}]_T$, and $[\bar{1}\bar{1}\frac{1}{2}]_T$ are equivalent. These twin laws are characterized by a small value of the obliquity (0·05°); therefore the individuals twinned by these laws generate reflections which, in the case of $l_T = 2n$, are almost exactly superposed on each other. A spot having film coordinates hkl is formed by the superposition of three reflections, one from each individual of the twin. On the other hand the superstructure reflections with $l_T = 2n+1$ of the different twin individuals do not overlap; therefore, by measuring equivalent superstructure reflections with $l_T = 2n+1$, the volume of each individual case can be determined. This allows the correction for twinning.

Electron diffraction photographs of the erbium–rhodium stannide, taken with a JEM-100CX of the DMG/CEN at Grenoble, did not show any evidence of twin lattices. All the spots could be indexed on a single tetragonal cell $a_{II} \times a_{II} \times c_{II}$. The images corresponded to sample sections of about 10–100 μm^2. These observations indicated that the samples examined by electron diffraction were either untwinned or, if twinned, each individual was larger than 10–100 μm^2.

Precession photographs of the 0,1,2,4,6 layers perpendicular to the $[001]_c$ direction and the 0,1,2,3,4,6 layers perpendicular to the $[111]_c$ direction were taken with Zr-filtered Mo $K\alpha$ radiation. All crystals were originally twinned with individuals contributing equally. However, grinding them into spheres changed the ratios of the different individuals which allowed the determination of the space group. The systematic absences were: for $(hkl)_T$ reflections $h+k+l = 2n+1$, for $(hk0)_T$ $h = 2n+1$, for $(h0l)_T$ or $(0kl)_T$ $l = 2n+1$, and for $(hhl)_T$ $2h+l \neq 4n$. These absences and the equivalence in intensity between Freidel's pairs and $(hkl)_T$ and $(khl)_T$ ones indicated that the probable space group was $I4_1/acd$.

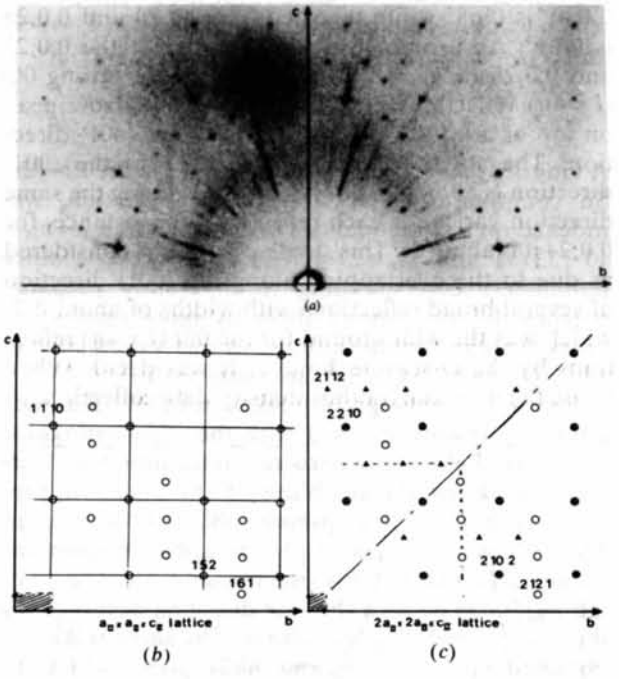

Fig. 1. $(2kl)_c$ layer of the pseudocubic $2a_{II} \times 2a_{II} \times c_{II}$ lattice. (*a*) Experimental precession photograph. (*b*) Schematic representation of an untwinned lattice; the unit cell corresponds to the shaded area. (*c*) Schematic representation of a twinned lattice: two individuals related by the threefold axis [111] are shown. The first corresponds to open circles, and the second to black triangles. Note that $(abc)_1 \rightarrow (bca)_2$. The unit cell is shaded. A row parallel to the *c* axis for each individual is shown.

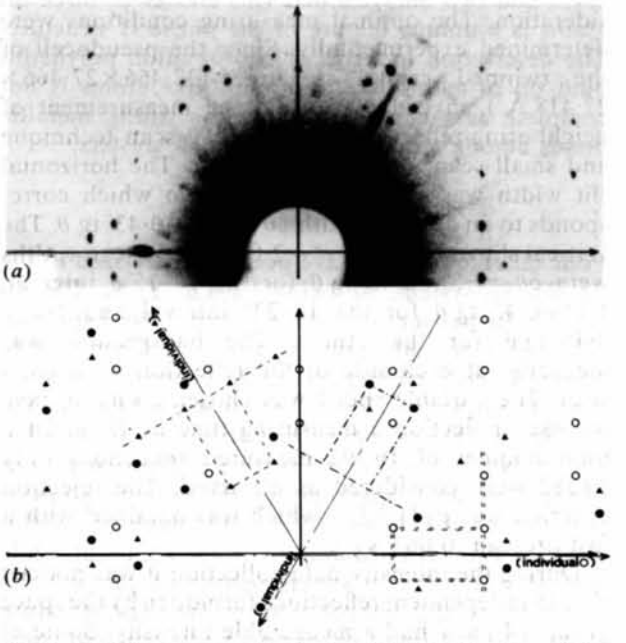

Fig. 2. Third layer perpendicular to the $[111]_c$ direction of the pseudocubic $2a_{II} \times 2a_{II} \times c_{II}$ lattice. (*a*) Experimental precession photograph. (*b*) Schematic representation of a twinned lattice: three individuals related by a pseudo threefold axis [111], the lattices of each individual are outlined differently.

Intensity data and corrections

The crystal used for the intensity-data collection was twinned. However, a large fraction of the different twin individuals were eliminated by grinding the crystal into a small sphere [$R = 0{\cdot}0081\,(7)$ cm]. This sphere was mounted on an automatic Nonius diffractometer equipped with a graphite monochromator and Ag $K\alpha$ radiation. In order to determine the percentage of each individual the intensities of three sets of 48 pseudo-equivalent superstructure reflections were measured. These reflections were $(18,4,3)_c$, $(12,2,3)_c$, and $(4,2,11)_c$. For each set of 48 reflections the 16 corresponding to one given individual always had zero intensity. This observation together with the long-exposure precession photographs indicated that the crystal studied consisted of only two individuals. From the intensity ratio it was determined that the two individuals occupied 94·8 (8) and 5·2 (5)% of the crystal volume, respectively. For the intensity-data collection only the reflections of the tetragonal cell $a_{II} \times a_{II} \times c_{II}$ coming from the strongest individual were measured. It must be pointed out that this compound could crystallize with the structure of phase III. It was not possible to eliminate the amount of this phase in our sample, but it could be estimated that it was less than a few per cent.

For the 10–15°θ interval all possible reflections were measured, whereas for the 3–10 and 15–23°θ intervals the measurements were limited to those with $l \geq 0$. For each interval only those reflections satisfying the condition $h+k+l=2n$ were taken into consideration. The optimal measuring conditions were determined experimentally. Since the pseudocell of the twinned crystal is large ($27{\cdot}466 \times 27{\cdot}466 \times 27{\cdot}418$ Å^3), in order to avoid the measurement of neighboring-reflection tails, the θ/θ scan technique and small scan widths were chosen. The horizontal slit width was $e' = (1{\cdot}5 + 1{\cdot}3 \text{ tg } \theta)$ mm which corresponds to an angular width $\delta\theta = 0{\cdot}5° + 0{\cdot}43° \text{ tg } \theta$. The vertical slit was fixed at $e'' = 2{\cdot}0$ mm. The scan widths were $\delta\theta = 1{\cdot}5° + 0{\cdot}45° \text{ tg } \theta$ for the 10–15°θ interval, $1{\cdot}1° + 0{\cdot}45° \text{ tg } \theta$ for the 18–23° interval and $1{\cdot}0° + 0{\cdot}45° \text{ tg } \theta$ for the others. The background was measured at each side of the reflection by a $\delta\theta/4$ scan. The variable speed was chosen so as to have for each reflection a measuring time of 180 s. Of a total number of 16 992 measured reflections only 10 582 were considered as observed. The rejection criterion was $\sigma(I) > I/2$ which was obtained with a fast prescan ($0{\cdot}067° \text{ s}^{-1}$).

During the intensity-data collection it was noticed that 15 independent reflections forbidden by the space group $I4_1/acd$ had a measurable intensity. Some of these extremely weak reflections were: 0,0,34; 0,0,18; 0,0,26; 006; $3\bar{3}0$; 13,$\bar{1}\bar{3}$,0; 0,13,$\bar{1}\bar{3}$; 17,17,0; 17,0,17.... In order to prove that they were not due to multiple diffraction, these reflections were remeasured with the θ/θ scan technique and Mo $K\alpha$ radiation at different ψ values. Their net intensity varied between I_{BG} and $I_{BG}/5$ (I_{BG} being the intensity of the background during the same time). Each net intensity did not vary with the ψ angle, which proved that the measurable intensity was not due to multiple diffraction. In addition, reflections not allowed by the I centering and having about the same intensity were observed. They were reflections such as 0,0,13; 0,0,17; 0,0,23; 0,0,25; 0,0,31; and 0,0,33; namely all belonging to the 00l row. Thus, all 00l reflections were measured by different types of scans, *i.e.* ω, θ/θ, and $\theta/2\theta$ scans for $\theta < 30°$. For the allowed reflections the half-intensity width with the three scan techniques varied between 0·3 and 0·7°, whereas much larger differences were obtained for the forbidden reflections. With the ω-scan technique, which corresponds to a scan perpendicular to the $\langle 00l \rangle$ direction, the width was constant (~0·4°) for all 00l reflections. Small tails were observed on each side of the very strong 00l (with $l = 4n$) reflections so that the base widths of these reflections were >0·7° (Fig. 3). With the θ/θ–scan technique all reflections had about the same width, *i.e.* 0·7° (Fig. 3). With the $\theta/2\theta$–scan technique, the strong 00l ($l = 4n$) reflections were very broad which did not allow separation between a given 00l reflection and the adjacent 00$l+1$ reflection. For instance, the angular separation between 0,0,48 and 0,0,47 is 0·65° while that between 0,0,24 and 0,0,25 is 0·61°. An example of a $\theta/2\theta$ scan for the 0,0,23 and 0,0,28 range is shown in Fig. 3. The strong 00l ($l = 4n$) reflections consist of a strong narrow peak on top of a diffuse streak parallel to the $\langle 001 \rangle$ direction. The streak width perpendicular to the $\langle 001 \rangle$ direction is about 0·7° while its length along the same direction varies for each reflection. For instance, for 0,0,24 it is about 2°. This streak can also be considered as due to the overlapping along the $\langle 001 \rangle$ direction of several broad reflections with widths of about 0·7° which was the width found for the 00l ($l = 4n$) reflections by the ω-scan technique. It was decided then to use the θ/θ scan for the intensity-data collection.

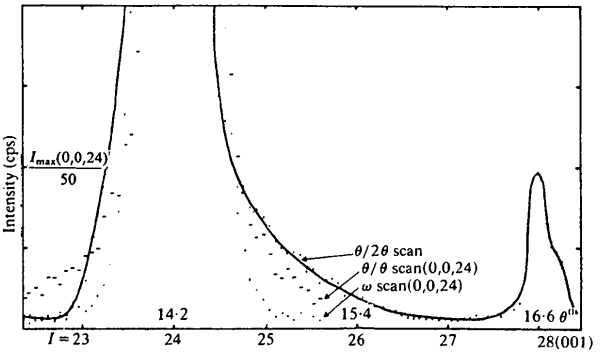

Fig. 3. Net intensities with different scan techniques of the 0,0,24 reflection: ω scan: black dots; θ/θ scan: horizontal dashes; $\theta/2\theta$ scan: black dots fitted by an experimental curve.

As has been stated above, the crystal used for the intensity-data collection was twinned and comprised two individuals. If *hkl*'s and *HKL*'s are the reflections of the largest (*A*) and the smallest (*B*) individuals, respectively, the two sets of reflections are related by the matrix:

$$\begin{pmatrix} H \\ K \\ L \end{pmatrix}_B = \begin{pmatrix} 0 & 1 & 0 \\ 0 & 0 & \frac{1}{2} \\ 2 & 0 & 0 \end{pmatrix} \begin{pmatrix} h \\ k \\ l \end{pmatrix}_A .$$

The intensity of a given *hkl* reflection is therefore:

$$I_{\text{total}}(hkl) = I_A(hkl) + I_B(k,l/2,2h).$$

Overlapping occurs only for $l = 2n$, namely for the pseudocubic reflections. If R is the ratio between the volume of the B and A individuals ($R = 5{\cdot}2/94{\cdot}8$), then the total intensity is given by:

$$I_{\text{total}}(hkl) = I_A(hkl) + RI_A(k,l/2,2h);$$

from which

$$\begin{aligned} I_A(hkl) &= I_{\text{total}}(hkl) - R[I_{\text{total}}(k,l/2,2h) \\ &\quad - RI_A(l/2,h,2k)] \\ &= I_{\text{total}}(hkl) - RI_{\text{total}}(k,l/2,2h) \\ &\quad + R^2 I_{\text{total}}(l/2,h,2k) - R^3 I_{\text{total}}(hkl) + \ldots . \end{aligned}$$

Since *hkl*; *k,l/2,2h*; *l/2,h,2k* are pseudo-equivalent reflections of the pseudocubic cell $a_{II} \times a_{II} \times c_{II}/2$ and their intensity does not vary by more than 5%, we can write:

$$\begin{aligned} I_A(hkl) &= I_{\text{total}}(hkl) - (R - R^2 + R^3 \\ &\quad - \cdots) I_{\text{total}}(k,l/2,2h) \\ &\simeq \frac{1}{(1+R)} I_{\text{total}}(hkl). \end{aligned}$$

These 3571 reflections, together with the superstructure ones (7011) for which overlapping does not occur, were used for the solution of the structure and the subsequent refinements. For the centrosymmetric point group $4/mmm$ there were 1163 independent reflections. All reflections satisfied the condition $F \geq 0{\cdot}02F_{\max}$ which corresponds to $I_{\text{NET}} \geq I_{\text{BG}}/2$. The average standard deviation calculated for each set of equivalent reflections showed that this relatively large value was probably due to a departure of the sample from spherical shape (~10%) which led to an absorption-correction error ($\mu = 193\ \text{cm}^{-1}$). The average difference in intensity between Friedel pairs (1%) was less than that due to the absorption-correction error. This indicated that the most probable space group was the centrosymmetric one. As has been stated, the strong streaks on each side of the strong reflections could be explained as being due to a convolution of forbidden, weak and broad reflections. By taking these reflections as observed, point groups of lower symmetry were tried. After averaging in the noncentrosymmetric point group $4mm$, the total number of independent reflections was reduced to 1434. Each reflection represents the average of at least four which are equivalent. For the point group $\bar{4}$ there were 3922 independent reflections with $F \geq 2\%\ F_{\max}$, each corresponding to the average of at least two observed reflections. In each case the integrated intensities were converted into structure factors by applying the Lorentz, polarization, and absorption ($\mu R = 1{\cdot}56$) corrections. Since the lattice parameters of these compounds vary from one batch to another, a measurement was made directly on the sphere used for the intensity-data collection. The θ and $-\theta$ values for 10 reflections in the range $\theta = 11$–$30°$ were measured with the four-circle diffractometer equipped with Ag $K\alpha$. For each reflection all the equivalent ones were measured. By using the Nelson–Riley and the Taylor–Sinclair extrapolation functions, the values $a_{II} = 13{\cdot}729\ (2)$ and $c_{II} = 27{\cdot}395\ (6)$ Å were obtained. The lattice parameters, as determined from Guinier powder data, corresponding to the batch from which the crystal had been taken, were $a_{II} = 13{\cdot}733\ (1)$ and $c_{II} = 27{\cdot}418\ (3)$ Å.

Solution of the structure

The formula, obtained by chemical analysis was $ErRh_{1{\cdot}1}Sn_{3{\cdot}6}$. Since the observed density was $9{\cdot}1\ \text{g cm}^{-3}$ the probable formula per unit cell of space symmetry $I4_1/acd$ could be $Er_{40}Rh_{48}Sn_{144}$. Three-dimensional Patterson series and direct methods failed to give conclusive information for the determination of the structure. Since the diffraction patterns of the four different phases (I, I′, II, and III) are closely related to each other as far as the cell parameters and intensities are concerned, the first steps toward the solution of the structure were based on crystal-chemical considerations. For instance, phases I, I′, and III contain three-dimensional networks of $RhSn_6$ trigonal prisms and large sites formed by these networks. A similar arrangement of $RhSn_6$ trigonal prisms was found to exist in the Patterson series of phase II. Hereafter, numbers in brackets will denote crystallographically independent sites with similar chemical behavior. By placing 16 $Rh_{[1]}$ atoms in the *16-fold positions* ($00z$; $z \simeq \frac{1}{8}$), 32 $Rh_{[2]}$ *atoms in the* 32-fold positions (xyz; $x \simeq \frac{1}{4}$, $y \simeq z \simeq 0$), 32 Sn atoms in two sets of the 16-fold positions ($xx\frac{1}{4}$) [$Sn(3)_{[1]} \equiv x \simeq \frac{1}{6}$ and $Sn(3)_{[2]} \equiv x \simeq \frac{1}{3}$] and 96 Sn atoms in three sets of the general 32-fold positions {(xyz) [$Sn(3)_{[3]} \equiv x \simeq \frac{1}{3}$, $y \simeq 0$, $z \simeq \frac{1}{12}$; $Sn(3)_{[4]} \equiv x \simeq 0$, $y \simeq \frac{1}{3}$, $z \simeq \frac{1}{12}$; $Sn(2) \equiv x \simeq y \simeq 2z \simeq \frac{1}{12}$]}, we obtained a network of $RhSn_6$ prisms which was closely related to that of phase III and consistent with the Patterson series. The large holes formed by this network were filled with rare-earth and Sn atoms. From steric considerations, we placed eight Er(1) atoms in the cuboctahedral eightfold

positions ($00\frac{1}{4}$), 32 Er(2) atoms in the 32-fold positions (xyz; $x \simeq y \simeq -2z \simeq 0{\cdot}13$), and 16 Sn(4) atoms in the 16-fold positions ($\frac{1}{4}x\frac{1}{8}$; $x \simeq 0{\cdot}21$). The structural refinements as well as the data reduction were carried out by using the Enraf–Nonius *SDP* system program. The f curves for neutral Er, Rh, and Sn given in *International Tables for X-ray Crystallography* (1974) were used. An anomalous-dispersion correction was applied to all atoms; the coefficients were those of Cromer & Liberman (1970). The weighting scheme $w = 1/\sigma(F^2)$ (with a zero ignorance factor) was that of the *SDP* system. Several cycles of refinements with the space group $I4_1/acd$, during which the scale factor, 19 positional parameters, 49 anisotropic thermal parameters, and 9 occupancy factors were varied, yielded $R = 0{\cdot}102$ and $wR = 0{\cdot}057$. By comparing the F_o with the F_c it was noticed that the strong reflections occurring at low θ angle were affected by extinction. The reflections highly affected by extinction are the strong reflections with low θ angle which are mainly subcell reflections. We preferred to exclude them from the subsequent refinements rather than to correct them because of the large correlation between the extinction and twinning corrections. All those reflections with $\sin\theta/\lambda < 0{\cdot}35$ Å^{-1} and $I > I_{max}/2$ were eliminated. The subsequent refinements were based on 954 reflections. At this stage the R and wR factors were 0·057 and 0·055, respectively. When all occupancy factors were varied, only that of the Er(1) site decreased appreciably, which was interpreted as an indication that this site was occupied by a mixture of Sn and Er atoms, whereas the occupancy factors of all other sites remained close to unity within their respective standard deviations.

Although the equivalence in intensity between Friedel pairs indicated that the structure of phase II contained a center of symmetry, a refinement in the noncentrosymmetric space group $I4_1cd$ was tried. From the original 1434 independent reflections corresponding to the point group $4mm$, 268 which were affected by extinction were eliminated using the same criterion defined above. After convergence was attained for all 133 parameters varied, the R and wR factors decreased to 0·029 and 0·028, respectively. The positions for all atoms, except Sn(4), remained close to the centrosymmetric ones within their respective standard deviations. The largest difference with respect to the centrosymmetric refinement was in the orientation of the thermal ellipsoid for the Sn(4) atom, accompanied by a small shift of its positional parameters. However, this shift was ~0·1 Å, while the largest axis of the thermal ellipsoid was always ~0·3 Å. The thermal ellipsoid of Sn(4) did not have any constraint in the space group $I4_1cd$, whereas it had $\beta_{12} = \beta_{13} = 0$ in $I4_1/acd$. A refinement carried out in the centrosymmetric space group without the constraints for Sn(4) gave 0·033 and 0·031 for the R and wR factors, respectively, and the standard deviations of all parameters were of the same order of magnitude as those obtained for the noncentrosymmetric $I4_1cd$. As stated above, weak and diffuse streaks appeared near the strong reflections, such as 0,0,12, 0,0,24, 12,12,0, *etc.*... These streaks, which were ~100 times weaker than the reflections, broke all extinction rules due to the a, c, d glides, the 4_1 screw axis, and the I centering. If these streaks are taken into account, the space symmetry of phase II cannot be higher than $P\bar{4}$. Since the intensity measurements were made by excluding those reflections for which $h+k+l = 2n+1$ and the diffuse streaks which broke this rule were few, only the I space groups were tried. No improvement was obtained with the space groups $I\bar{4}2m$ and $I4_122$. The best results were obtained with $I4_1$ and $I\bar{4}$. However, large correlations existed among the thermal parameters. In the latter space group there were 3922 independent reflections, which were reduced to 3234 by the extinction-correction criterion ($\sin\theta/\lambda < 0{\cdot}35$ Å^{-1} and $I > I_{max}/2$), and 265 positional and anisotropic thermal parameters. The R and wR factors were 0·034 and 0·033, respectively. The final positional parameters were very close to those obtained with the space group $I4_1/acd$. For instance, the shift of the Sn(4) atoms from the centrosymmetric special positions was less than 0·005 Å while the major axis of their thermal ellipsoid was still 0·3 Å. An interesting feature for the space group $I\bar{4}$ was that it allowed a partial ordering of the Sn and Er atoms over the $M(1)$ sites. In the space groups $I4_1/acd$ and $I4_1cd$ these sites ($00\frac{1}{4}$) have an eightfold multiplicity; whereas they split into two sets of four positions in the space group $I\bar{4}$: ($00z$; $z \sim \frac{1}{4}$) and ($0\frac{1}{2}z$; $z \sim 0$), respectively. As obtained from the refinement, the former contains (0·67 Er + 0·33 Sn) and the latter only Sn atoms. If one considered the space group $P\bar{4}$, the $M(1)$ site would split into four different twofold positions which would allow a more perfect ordering (Fig. 4). Therefore, the diffuse streaks near the strong reflections are due to a short-range order taking place over the $M(1)$ sites between the Sn and Er atoms. Although the R factors of the $I4_1/cd$ refinement are slightly smaller than those of $I4_1acd$, in *Discussion* we shall describe the structure of phase II as belonging to the centrosymmetric space group with a small departure for the orientation of the Sn(4) thermal ellipsoid. This choice is corroborated by the large correlations, obtained with the space group $I4_1cd$, between parameters of atoms related by the pseudocenter of symmetry.

The final positional and thermal parameters are given in Tables 1 and 2.* The occupancy factor of

* A list of structure factors has been deposited with the British Library Lending Division as Supplementary Publication No. SUP 38753 (6 pp.). Copies may be obtained through The Executive Secretary, International Union of Crystallography, 5 Abbey Square, Chester CH1 2HU, England.

Table 1. *Positional, occupancy, and thermal parameters*

$M(1) \equiv [Sn(1)_xEr(1)_{1-x}]$; $x = 0{\cdot}68$ (2).

	Position	Site symmetry	x	y	z	β_{11}	β_{22}	β_{33}	β_{12}	β_{13}	β_{23}
Er(1), Sn(1)	8(*b*)	222	0	0	$\frac{1}{4}$	0·00158 (8)	0·00158	0·00042 (2)	−0·0001 (1)	0	0
Er(2)	32(*g*)	1	0·13343 (5)	0·13765 (5)	−0·06842 (2)	0·00091 (2)	0·00102 (2)	0·00028 (1)	−0·00011 (4)	0·00007 (2)	−0·00007 (2)
Sn(2)	32(*g*)	1	0·08725 (8)	0·08851 (8)	0·04409 (3)	0·00139 (4)	0·00142 (4)	0·00038 (1)	0·00108 (7)	0·00054 (4)	0·00055 (4)
$Sn(3)_{[1]}$	16(*f*)	2	0·1765 (1)	0·1765	$\frac{1}{4}$	0·00087 (6)	0·00087	0·00125 (2)	0·0005 (1)	−0·0003 (1)	0·0003
$Sn(3)_{[2]}$	16(*f*)	2	0·3266 (1)	0·3266	$\frac{1}{4}$	0·00097 (7)	0·00097	0·00132 (2)	0·0005 (1)	−0·0005 (1)	0·0005
$Sn(3)_{[3]}$	32(*g*)	1	0·32578 (8)	0·00919 (9)	0·08708 (4)	0·00095 (4)	0·00333 (6)	0·00029 (1)	−0·00071 (9)	−0·00033 (4)	0·00039 (5)
$Sn(3)_{[4]}$	32(*g*)	1	0·0047 (1)	0·32420 (9)	0·08723 (5)	0·00530 (8)	0·00102 (5)	0·00024 (1)	−0·0011 (1)	−0·00037 (5)	−0·00028 (4)
Sn(4)	16(*e*)	2	$\frac{1}{4}$	0·2111 (1)	$\frac{1}{8}$	0·0068 (1)	0·00141 (7)	0·00145 (3)	−0·0038 (4)	0·00467 (8)	0·0001 (4)
$Rh_{[1]}$	16(*d*)	2	0	0	0·12245 (5)	0·00063 (6)	0·00059 (5)	0·00024 (1)	−0·0001 (1)	0	0
$Rh_{[2]}$	32(*g*)	1	0·24391 (6)	0·00120 (8)	−0·0001 (1)	0·00077 (3)	0·00061 (3)	0·00019 (1)	−0·00003 (8)	0·0000 (2)	−0·00005 (4)

the $M(1)$ site, assuming that it was fully occupied by Sn atoms, was 1·116(6) which corresponded approximately to $[Er(1)_{1/3}Sn(1)_{2/3}]$. The thermal parameters of the Sn(4) atoms correspond to those obtained without the constraint $\beta_{12} = \beta_{13} = 0$. The positional parameters together with the unit-cell dimensions as determined by X-ray powder data gave the interatomic distances reported in Table 3.

Discussion

The X-ray structural analysis showed that phase II of the Er–Rh–Sn compound has the following chemical formula: $[Sn(1)_{2/3}Er(1)_{1/3}]Er(2)_4Rh_6Sn(2)_4Sn(3)_{12}Sn(4)_2$ where Sn(3) and Rh correspond to four and two different crystallographic sites, respectively. There are eight formulae per unit cell. This X-ray formula ($ErRh_{1.39}Sn_{4.32}$) is not in good agreement with that determined by chemical analysis ($ErRh_{1.1}Sn_{3.6}$). The compositions corresponding to full occupancy of site (1) by either Sn(1) or Er(1) are $ErRh_{1.5}Sn_{4.75}$ or $ErRh_{1.2}Sn_{3.6}$, respectively. The chemical analysis probably corresponds to a sample with a composition closer to the latter. The importance of the stoichiometry variation has been pointed out by Ott *et al.* (1980) who have shown that two samples prepared with nominal Er/Rh ratios equal to 1·0 and 0·5 have different properties. For instance, the first does not become superconducting and shows only a magnetic ordering at 0·65 K, while the second is a reentrant superconductor with $T_c = 1{\cdot}05$ and $T_m = 0{\cdot}5$ K. An increase of Er atoms in the structure corresponds to an increase of magnetic interactions which at a given concentration prevent the compound from becoming superconducting.

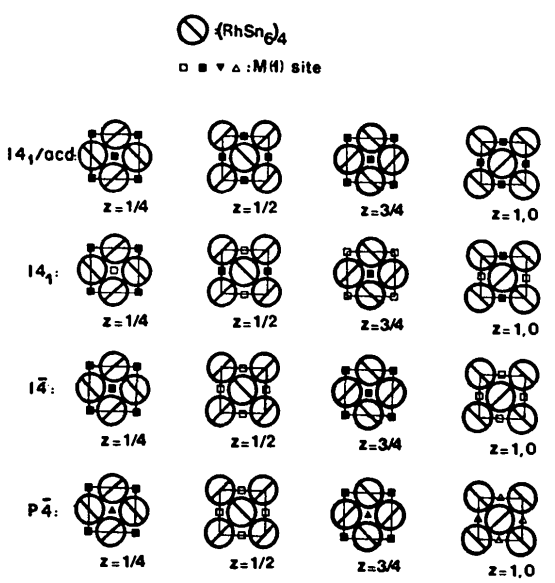

Fig. 4. Schematic representation of the ordering for the $M(1)$ site for different space groups. For $I4_1/acd$ all sites are equivalent. For the others, the inequivalent sites are represented by different symbols. The symbol representing the $(RhSn_6)_4$ group is the same as that shown in Fig. 8.

Table 2. *Thermal data*

			Angle (°) with x	y	z
Er(1), Sn(1)	*r*1	0·126 Å	90	90	0
	*r*2	0·125	45	135	90
	*r*3	0·121	45	45	90
Er(2)	*r*1	0·106	72·1	117·7	33·9
	*r*2	0·097	97·6	32·5	58·5
	*r*3	0·092	19·6	74·3	101·4
Sn(2)	*r*1	0·155	56·2	55·2	52·8
	*r*2	0·094	112·9	117·6	37·3
	*r*3	0·091	42·8	132·7	92·0
$Sn(3)_{[1]}$	*r*1	0·219	94·0	86·0	5·7
	*r*2	0·104	45	45	90
	*r*3	0·074	134·7	45·3	95·7
$Sn(3)_{[2]}$	*r*1	0·226	96·1	83·9	8·6
	*r*2	0·108	45	45	90
	*r*3	0·076	45·6	134·4	81·4
$Sn(3)_{[3]}$	*r*1	0·182	99·3	14·3	79·3
	*r*2	0·110	123·7	104·2	37·3
	*r*3	0·082	35·3	88·6	57·8
$Sn(3)_{[4]}$	*r*1	0·227	7·9	96·6	94·3
	*r*2	0·110	88·1	43·9	133·8
	*r*3	0·077	82·2	46·9	44·1
Sn(4)	*r*1	0·327	41·4	97·9	49·7
	*r*2	0·163	115·1	49·5	58·9
	*r*3	0·024	59·6	41·6	115·4
$Rh_{[1]}$	*r*1	0·096	90	90	0
	*r*2	0·079	30·1	120·1	90
	*r*3	0·074	59·9	30·1	90
$Rh_{[2]}$	*r*1	0·086	50·0	105·8	44·3
	*r*2	0·086	40·4	82·6	129·4
	*r*3	0·075	85·4	17·6	73·1

Table 3. *Interatomic distances* (Å)

Coordination polyhedra ($d \leq 4{\cdot}35$ Å)

$Sn(3)_{[1]}$ site	
$Sn(3)_{[1]}$–Rh_2 ×2	2·644 (1)
$Sn(3)_{[1]}$–Er(2) ×2	3·2586 (7)
–$M(1)$	3·4273 (8)
$Sn(3)_{[1]}$–$Sn(3)_{[2]}$	2·916 (1)
–$Sn(3)_{[3]}$ ×2	3·313 (1)
–$Sn(3)_{[4]}$ ×2	3·451 (1)
–Sn(2) ×2	3·6673 (8)
–Sn(4) ×2	3·604 (1)
$Sn(3)_{[3]}$ site	
$Sn(3)_{[3]}$–$Rh_{[1]}$	2·640 (1)
–$Rh_{[2]}$	2·645 (2)
$Sn(3)_{[3]}$–Er(2)	3·282 (1)
–Er(2)	3·287 (1)
–$M(1)$	3·382 (1)
$Sn(3)_{[3]}$–$Sn(3)_{[3]}$	2·942 (2)
–$Sn(3)_{[1]}$	3·313 (1)
–$Sn(3)_{[2]}$	3·462 (1)
–$Sn(3)_{[4]}$	3·357 (1)
–$Sn(3)_{[4]}$	3·446 (1)
–Sn(2)	3·648 (1)
–Sn(2)	3·637 (1)
–Sn(4)	3·138 (2)
–Sn(4)	4·350 (2)
Sn(2) site	
Sn(2)–$Rh_{[1]}$	2·7440 (8)
–$Rh_{[2]}$	2·745 (1)
–$Rh_{[2]}$	2·735 (1)
Sn(2)–Er(2)	3·2207 (7)
–Er(2)	3·2195 (8)
–Er(2)	3·1960 (8)
Sn(2)–Sn(2)	3·414 (1)
–Sn(2) ×2	3·416 (1)
–$Sn(3)_{[1]}$	3·667 (1)
–$Sn(3)_{[2]}$	3·681 (1)
–$Sn(3)_{[3]}$	3·648 (1)
–$Sn(3)_{[3]}$	3·637 (1)
–$Sn(3)_{[4]}$	3·628 (1)
–$Sn(3)_{[4]}$	3·690 (1)
–Sn(4)	3·571 (1)
$Rh_{[1]}$ trigonal prism	
$Rh_{[1]}$–$Sn(3)_{[3]}$ ×2	2·640 (1)
–$Sn(3)_{[4]}$ ×2	2·656 (1)
–Sn(2) ×2	2·7440 (8)
$Rh_{[1]}$–Er(2) ×2	3·0209 (5)
–$M(1)$	3·4971 (8)
$Rh_{[2]}$ trigonal prism	
$Rh_{[2]}$–$Sn(3)_{[1]}$	2·644 (1)
–$Sn(3)_{[2]}$	2·653 (1)
–$Sn(3)_{[3]}$	2·645 (2)
–$Sn(3)_{[4]}$	2·631 (2)
–Sn(2)	2·745 (1)
–Sn(2)	2·735 (1)
$Rh_{[2]}$–Er(2)	3·052 (1)
–Er(2)	3·013 (1)
–$M(1)$	3·517 (1)

$Sn(3)_{[2]}$ site	
$Sn(3)_{[2]}$–$Rh_{[2]}$ ×2	2·653 (1)
$Sn(3)_{[2]}$–Er(2) ×2	3·2489 (7)
–$M(1)$	3·3671 (8)
$Sn(3)_{[2]}$–$Sn(3)_{[1]}$	2·916 (1)
–$Sn(3)_{[3]}$ ×2	3·462 (1)
–$Sn(3)_{[4]}$ ×2	3·330 (1)
–Sn(2) ×2	3·6815 (9)
–Sn(4) ×2	3·921 (1)
$Sn(3)_{[4]}$ site	
$Sn(3)_{[4]}$–$Rh_{[1]}$	2·656 (1)
–$Rh_{[2]}$	2·631 (2)
$Sn(3)_{[4]}$–Er(2)	3·309 (1)
–Er(2)	3·220 (1)
–$M(1)$	3·399 (1)
$Sn(3)_{[4]}$–$Sn(3)_{[4]}$	2·909 (2)
–$Sn(3)_{[1]}$	3·451 (1)
–$Sn(3)_{[2]}$	3·330 (1)
–$Sn(3)_{[3]}$	3·357 (1)
–$Sn(3)_{[3]}$	3·446 (1)
–Sn(2)	3·628 (1)
–Sn(2)	3·690 (1)
–Sn(4)	3·852 (2)
–Sn(4)	3·679 (2)
Sn(4) site	
Sn(4)–Er(2) ×2	3·057 (1)
Sn(4)–$Sn(3)_{[3]}$ ×2	3·138 (2)
Sn(4)–Sn(2) ×2	3·571 (1)
–$Sn(3)_{[1]}$ ×2	3·604 (1)
–$Sn(3)_{[2]}$ ×2	3·921 (1)
–$Sn(3)_{[4]}$ ×2	3·852 (2)
–$Sn(3)_{[4]}$ ×2	3·679 (2)
–$Sn(3)_{[3]}$ ×2	4·350 (2)
$M(1)$ cuboctahedron	
$M(1)$–$Sn(3)_{[1]}$ ×2	3·4273 (8)
–$Sn(3)_{[2]}$ ×2	3·3671 (8)
–$Sn(3)_{[3]}$ ×4	3·382 (1)
–$Sn(3)_{[4]}$ ×4	3·399 (1)
$M(1)$–$Rh_{[1]}$ ×2	3·4971 (8)
–$Rh_{[2]}$ ×4	3·5170 (6)
Er(2) truncated cuboctahedron	
Er(2)–Sn(2)	3·2207 (7)
–Sn(2)	3·1960 (8)
–Sn(2)	3·2195 (8)
–$Sn(3)_{[1]}$	3·2586 (6)
–$Sn(3)_{[2]}$	3·2489 (9)
–$Sn(3)_{[3]}$	3·282 (1)
–$Sn(3)_{[3]}$	3·286 (1)
–$Sn(3)_{[4]}$	3·309 (1)
–$Sn(3)_{[4]}$	3·220 (1)
–Sn(4)	3·057 (1)
Er(2)–$Rh_{[1]}$	3·0209 (6)
–$Rh_{[2]}$	3·052 (1)
–$Rh_{[2]}$	3·013 (1)

Er–Er separations ($d < 7{\cdot}0$ Å)

Er(2)–Er(2)	4·3759 (9)
Er(2)–Er(2) ×2	5·2857 (8)
–Er(2)	5·2655 (8)
Er(2)–Er(2)	5·8456 (8)
–Er(2)	5·8174 (8)
–$M(1)$	5·6318 (6)
	5·6248 (6)
	5·6952 (6)
$M(1)$–Er(2) ×4	5·6318 (6)
–Er(2) ×4	5·6248 (6)
–Er(2) ×4	5·6952 (6)

The 128 Sn atoms corresponding to sites (2), $(3)_{[1]}$, $(3)_{[2]}$, $(3)_{[3]}$, and $(3)_{[4]}$ have the same chemical behavior as they form a three-dimensional array of trigonal prisms whose centers are occupied by the $Rh_{[1]}$ and $Rh_{[2]}$ atoms. As can be seen from Fig. 5 the $Rh_{[2]}$ atoms form slightly distorted square lattices parallel to the (001) plane with a lattice parameter of $\sqrt{2}\, a_{II}/4$, and located at $z = 0, \frac{1}{4}, \frac{1}{2}, \frac{3}{4}$. The $Rh_{[1]}$ atoms also form square lattices parallel to the (001) plane, but with a different lattice parameter, $a_{II}/2$. They are located at $z = \frac{1}{8}, \frac{3}{8}, \frac{5}{8}$, and $\frac{7}{8}$, namely in between the square lattices formed by the $Rh_{[2]}$ atoms. The $Rh_{[1]}$ and $Rh_{[2]}$ atoms together form a distorted three-dimensional array of corner-sharing octahedra. The Sn prism around the $Rh_{[2]}$ atoms forms corner-sharing layers (A); that at $z = 0$ is shown in Fig. 6(a). The layers at $z = \frac{1}{4}, \frac{1}{2}, \frac{3}{4}$, and 1 are obtained from this by subsequent origin translations of $(\frac{1}{2}00)$, $(0\frac{1}{2}0)$, $(-\frac{1}{2}00)$, and $(0-\frac{1}{2}0)$, respectively, or by a rotation around the 4_1 screw axis placed at $(\frac{1}{4}\frac{1}{4}z)$ or an equivalent one at $(\frac{1}{4}\frac{3}{4}z)$, $(\frac{3}{4}\frac{1}{4}z)$, and $(\frac{3}{4}\frac{3}{4}z)$. On the other hand, the Sn prisms around $Rh_{[1]}$ form layers (B) of isolated prisms, as they do not share any vertices among themselves. The layer at $z = \frac{1}{8}$ is shown in Fig. 6(b). They share, instead, all their vertices with the prisms of the (A) layers above and below (Fig. 7a). The isolated-prism layers at $z = \frac{3}{8}, \frac{5}{8}, \frac{7}{8}$, and $\frac{9}{8}$ are obtained from that at $z = \frac{1}{8}$ by successive 90° rotations around the 4_1 screw axis at $(\frac{1}{4}\frac{1}{4}z)$ or equivalent ones at $(\frac{1}{4}\frac{3}{4}z)$, $(\frac{3}{4}\frac{1}{4}z)$, and $(\frac{3}{4}\frac{3}{4}z)$.

The arrangement of corner-sharing prism layers intercalated with isolated-prism layers exists also perpendicularly to the [100] (or [010]) direction. The corner-sharing prism layers are located at $x = 0$ and $\frac{1}{2}$ (or $y = 0$ and $\frac{1}{2}$) while the isolated-prism layers are located at $x = \frac{1}{4}$ and $\frac{3}{4}$ (or $y = \frac{1}{4}$ and $\frac{3}{4}$). It is evident that the layers perpendicular to the [100] (or [010]) direction are different from those perpendicular to the [001] direction (Fig. 7a, b).

The corner-sharing prism layers and the way they are stacked in the third dimension can be more precisely described if one takes as the basic unit the planar four-prism ring (star), shown as shaded in Fig. 6(a), instead of a single prism. Corner-sharing prism layers become corner-sharing star layers. For the

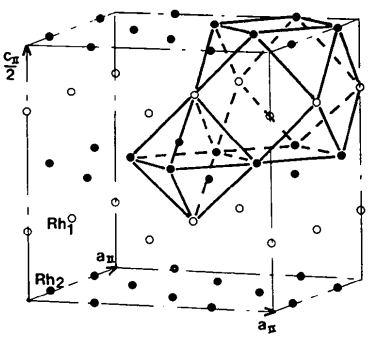

Fig. 5. Three-dimensional representation of the Rh sublattice.

layers parallel to the *ab* plane, a star of a given layer is related to the adjacent ones of the same layer by a rotation of $\pi/2$. In the structure of phase I there also exist corner-sharing star layers. However, in this case all the stars of a given layer are identical, while the relationship between any given star and the adjacent one along the third dimension is a rotation of $\pi/2$ around an axis placed at the center of the star and perpendicular to the layer (Fig. 8). This corresponds to an inversion of the star layers on going from any one layer to the next. In the structure of phase II the relationship between any star layer and an adjacent layer along the [001] direction consists of an origin shift of either $(0\frac{1}{2}0)$ or $(\frac{1}{2}00)$. It can be seen that in this case the stars form zigzag chains along the [001] axis. The isolated prisms join together the corner-sharing star layers. Fig. 8 shows the corner-sharing star layers perpendicular to the [100] (or [010]) direction.

Each of the $Sn(3)_{[1]}$ and $Sn(3)_{[2]}$ atoms is bonded to two $Rh_{[2]}$ atoms; therefore they belong to the corner-sharing prism layers (*A*). On the other hand, each of the $Sn(3)_{[3]}$ and $Sn(3)_{[4]}$ atoms is bonded to one $Rh_{[1]}$ and one $Rh_{[2]}$; they thus link together a corner-sharing prism layer (*A*) to an isolated-prism layer (*B*). Each Sn(2) atom is bonded to three Rh atoms, two $Rh_{[1]}$ and one $Rh_{[2]}$; and it is shared by two adjacent prisms of the same (*A*) layer and a prism of the (*B*) layer. If we consider only the Rh,

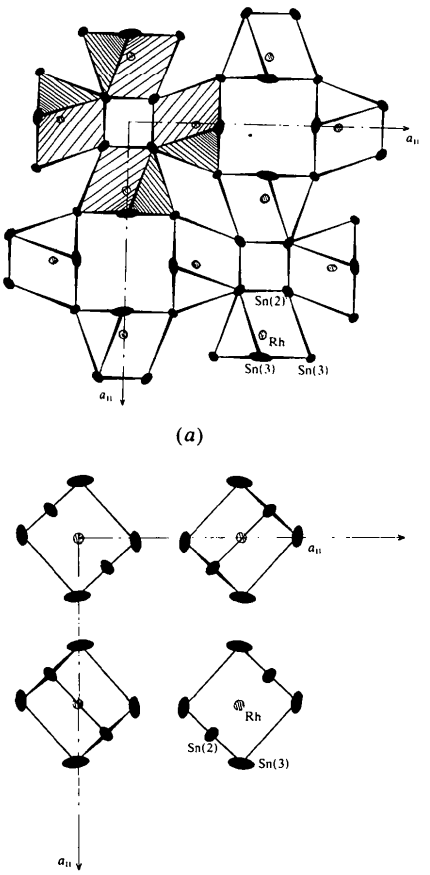

(*a*) (*b*)

Fig. 6. Projection on the (001) plane of the coordination polyhedra around the Rh atoms. The atoms are represented by the section of their thermal ellipsoid. (*a*) $z = 0$: corner-sharing Sn-prism layer; four Sn prisms forming a 'star' are shaded. (*b*) $z = \frac{1}{8}$: isolated Sn-prism layer.

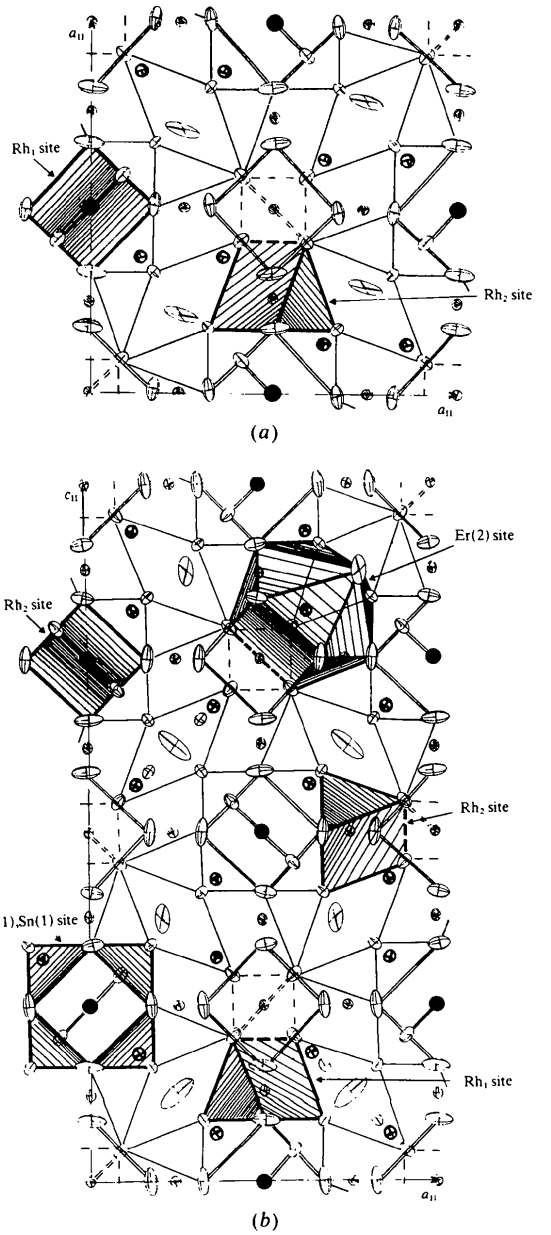

(*a*) (*b*)

Fig. 7. (*a*) Projection on the (001) plane of atoms with $-0{\cdot}05 < z < 0{\cdot}21$. One Sn prism around $Rh_{[1]}$ and $Rh_{[2]}$ is shaded. Prisms whose Rh is at $z = 0$ and $z = \frac{1}{8}$ are represented by single and double lines, respectively. The atoms are represented by their thermal ellipsoids. (*b*) Projection on the (010) plane of atoms with $-0{\cdot}09 < y < 0{\cdot}492$. The $Rh_{[1]}$, $Rh_{[2]}$, $M(1)$ and Er(2) coordination polyhedra are shaded. Prisms whose Rh is at $y = 0$ and $y = \frac{1}{4}$ are outlined by single and double lines, respectively.

Sn(2) and Sn(3) atoms, the chemical formula can be written as $(Rh_{[1]})_2(Rh_{[2]})_4Sn(2)_4$ $(Sn(3)_{[1]})_2(Sn(3)_{[2]})_2$ $(Sn(3)_{[3]})_4(Sn(3)_{[4]})_4$, or $Rh_6^{VI}Sn(2)_4^{III}Sn(3)_{12}^{II}$, in which the Roman numerals indicate the coordination numbers. The Rh and Sn(3) atoms form nearly cubic sublattices; the tetragonality is due to the positions occupied by the Sn(2) atoms. The pseudocubic $Rh_6Sn(3)_{12}$ framework forms three types of large holes, the first at the $8(b)(00\frac{1}{4})$ positions, the second at the $16(e)(\frac{1}{4}x\frac{1}{8}; x\sim\frac{1}{4})$ positions, and the third at the $8(a)(000)$ positions. The $8(b)$ holes, which have 222 point symmetry, are occupied by $M(1)$ atoms [randomly by Er(1) and Sn(1)]. The Sn(3) form around them slightly distorted cuboctahedra with an average $M(1)$–Sn(3) distance 3·393 Å. The Rh atoms form the second-nearest-neighbor polyhedron, namely an octahedron with an average $M(1)$–Rh distance 3·510 Å (see Fig. 5). Each Rh atom caps a rectangular face of the Sn cuboctahedron. The $16(e)(\frac{1}{4}\frac{1}{4}\frac{1}{8})$ holes are enclosed by 12 Sn(3) and 12 Rh atoms. These holes are very large [center–Sn(3) = 3·729 Å, center–Rh = 4·853 Å] so that they are occupied by three atoms, two Er(2) and one Sn(4). The $8(b)(00\frac{1}{4})$ positions, occupied by the $M(1)$ atoms, together with the empty $8(a)(000)$ sites define 16 subcubes whose edges are: $a_{II}/2$, $a_{II}/2$, $c_{II}/4$. The centers of these subcubes are the $16(e)(\frac{1}{4}\frac{1}{4}\frac{1}{8})$ positions. The 12 Sn(3) atoms, enclosing each of these positions, are placed two by two on the faces of the subcubes. Two Er(2) atoms are located in each subcube along its diagonals, toward the empty $8(a)$ corners and away from the $M(1)$ atoms (Fig. 9). There are four possible positions for the two Er atoms in each subcube, and in the unit cell there are eight possible orientations for the Er doublets. For instance, the two Er atoms, contained in the subcube around the $\frac{1}{4}\frac{1}{4}\frac{1}{8}$ position, move toward the $\frac{1}{2}\frac{1}{2}0$ and $0\frac{1}{2}\frac{1}{4}$ positions and the doublet is found at (0·362, 0·367, 0·068)–(0·138, 0·367, 0·182). This displacement of the Er atoms is needed in order to tilt the Sn(2) sublattice in such a way as to generate the prismatic framework. The Sn(3) sublattice forms only squares and it is the Sn(2) sublattice which transforms these squares into prisms (Fig. 6*b*). The thermal vibrations of these atoms are of the same order of magnitude as those of the corresponding atoms of phase I.

The Er(2) sites are enclosed by 10 Sn atoms. The corresponding polyhedra can be described as truncated cuboctahedra. If one looks down at a Sn cuboctahedron along one of its four threefold axes, there are three Sn atoms above, six at the same level as the central atom and three Sn atoms below. In the Sn polyhedra around the Er(2) atoms, either the three Sn atoms above or the three below are missing and replaced by one Sn(4) atom. The Er(2) atoms are displaced along the pseudo threefold axis so as to come in between the six Sn [*i.e.* Sn(3)] and the remaining three Sn atoms [*i.e.* Sn(2)], and away from the Sn(4) atom (Fig. 10). This atom is located near the $16(e)(\frac{1}{4}\frac{1}{4}\frac{1}{8})$ positions and in between two Er(2) atoms; it links, thus, two truncated cuboctahedra. The Sn(4) environment is very different from those of the Sn(1), Sn(2), and Sn(3) atoms, which have as first-nearest neighbors: 12 Sn + 6 Rh, 3 Er + 3 Rh, and 2 Er + 2 Rh + $M(1)$, respectively. The Sn(4) atoms are surrounded by 14 Sn and 2 Er atoms. However, the 14 Sn(4)–Sn distances vary over such a large range (3·138 to 4·350 Å) that it is difficult to decide the coordination number. The interatomic distances given in Table 3 indicate that it would be a good approximation to assign to the Sn(4) atoms a coordination number 12 [2 Er(2) + 2 Sn(2) + 8 Sn(3)]. Among these twelve atoms there are four which are relatively close [2 Er–Sn(4) = 3·057 Å and 2 Sn(3)–Sn(4) = 3·138 Å] and eight which are farther away. The four close atoms are in the same plane as Sn(4) itself (see Figs. 9 and 10) and form a rhombus around it. In the space group $I4_1/acd$ the site symmetry does not allow the Sn(4) atom to move out of the plane formed by

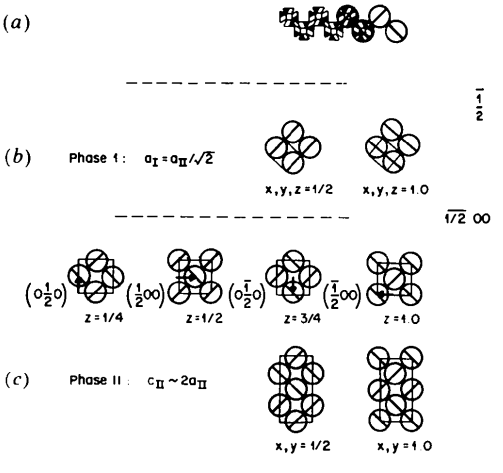

Fig. 8. (*a*) Schematic representation of $(RhSn_6)_4$ 'stars' as circles. Bisecting lines indicate prism tilt. (*b*) Star stacking in phase I. (*c*) Star stacking in phase II. The $\{\frac{1}{2}00\}$ vectors relating successive corner-sharing (001) layers are shown.

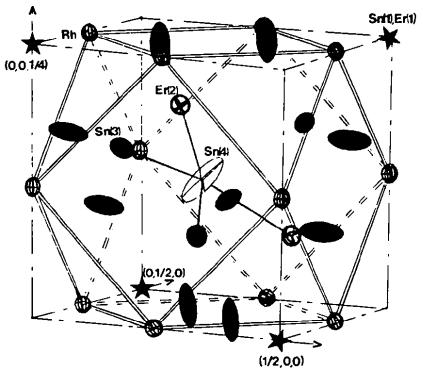

Fig. 9. $(\frac{1}{4}\frac{1}{4}\frac{1}{8})$ subcube occupied by two Er(2) and one Sn(4); the Rh cuboctahedron is represented by a double line, the short Sn(4)–Er(2), Sn(4)–Sn(3) bonds are represented by a single line.

2 Er(2)–2 Sn(3); however, a large thermal vibration perpendicular to this plane was obtained for Sn(4). The space group $I4_1/acd$ does not allow this orientation of the thermal ellipsoid either but, as has been stated above, the best refinement was obtained by removing the constraint $\beta_{12}=\beta_{13}=0$ for the Sn(4) atoms. The values $\beta_{12}=-0{\cdot}0038$, $\beta_{13}=0{\cdot}0047$ yielded by the refinement correspond to an angle of ~90° between the major axis of the thermal ellipsoid and the 2 Er(2)–2 Sn(3) plane (Fig. 10). Since the final positional parameters of Sn(4) obtained with the noncentrosymmetric space group $I4_1cd$ are very close to those obtained with the centrosymmetric one, this nonharmonic orientation is probably due to the short distances Sn(4)–Er(2) and Sn(4)–Sn(3) rather than to a static distortion.

The Er(2) sublattice forms distorted tetrahedra centered around the 8(*a*)(000) positions. Each face of these tetrahedra is capped with Sn(2) atoms, which are also arranged as distorted tetrahedra around the same positions. It is the arrangement of these interpenetrated tetrahedra which is responsible for the tetragonality of the structure (Fig. 11). The intratetrahedra Er(2)–Er(2) distances are about 5·28 Å, while each Er(2) is 'bonded' to another Er(2) of an adjacent tetrahedron by a distance of 4·376 Å. The Er(2) sublattice can be described either as a network of Er tetrahedra joined together by shorter Er–Er 'bonds', or as a network of isolated Er(2)–Er(2) doublets. This latter network is shown by thick lines in Fig. 11. The Er–Er doublets are related to each other by the 4_1 screw axis located at $(\frac{1}{4}\frac{1}{4}0)$ [or $(\frac{1}{4}\frac{3}{4}0)$, $(\frac{3}{4}\frac{1}{4}0)$, $(\frac{3}{4}\frac{3}{4}0)$]. Each doublet is formed by two Er atoms belonging to the same subcube.

Since the Er(2) and Sn(2) atoms form similar sublattices and the rest of the structure is pseudocubic, the two sublattices can interchange for each other and structures containing domains are obtained. The exchange between the two sublattices, which would take place at the domain walls, corresponds to changing the orientation of the unique fourfold axis from the [001] direction to either [100] or [010]. The same relationship exists among the different individuals of a twinned crystal; therefore the difference among these individuals is the interchange of the Er(2) sublattice with that of Sn(2), while the rest of the structure remains almost unchanged. The exchange is accompanied by displacements of about 1·10 Å for the positions of Er(2) and Sn(2) whereas Rh, Sn(1), Sn(3), and Sn(4) are displaced by less than 0·05, 0·00, 0·25, and 0·60 Å, respectively. The relatively large value for Sn(4) is due to the strong bonding existing between Er(2) and Sn(4). It can be seen from Fig. 12 that the diffuse streaks of phase III correspond to the superstructure reflection of phase II; the diffuse streaks are due, therefore, to a short-range order between the Er(2) and Sn(2) sublattices. This is corroborated by the large decrease in intensity observed when superstructure reflections of precession photographs for the Er and Sc compounds are compared.

In phase I (Hodeau *et al.*, 1980), the two types of Sn atoms have different chemical behavior; *i.e.* cation-like and anion-like. The chemical inequivalences of several Sn sites have been confirmed in the Er compound by Mössbauer data (Shenoy *et al.*, 1980). As far as chemical bonds are concerned, each of the $Sn(3)_{[1]}$, $Sn(3)_{[2]}$, $Sn(3)_{[3]}$ and $Sn(3)_{[4]}$ atoms forms identical bonds with the surrounding atoms (Table 3) and has an anion-like behavior. It should be pointed out that a short bond (2·922 Å) is found between two Sn(3) atoms. The same feature exists in phase I where two anion-like Sn atoms give rise to a distance of 2·967 Å. The anion-like behavior could also be attributed to Sn(2); however, these atoms have the property that they can be interchanged with the

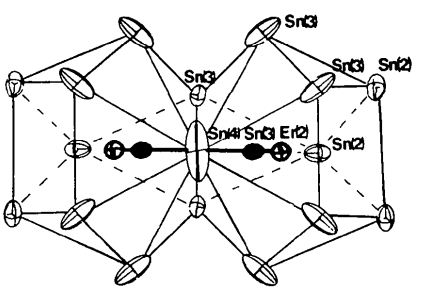

Fig. 10. Coordination Sn polyhedra of two Er(2) of the same subcube; these truncated cuboctahedra share a triangular face. The projection of the Sn(4) rhombus site Er(2) and 2 Sn(3) is represented by a thick line; these Sn(3) (black ellipses) do not belong to the coordination polyhedra shown in the figure.

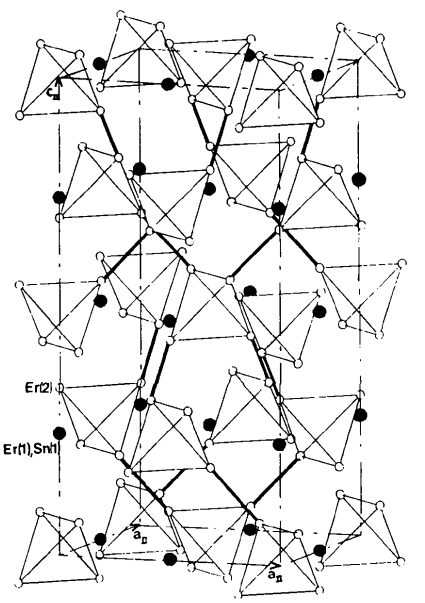

Fig. 11. Three-dimensional representation of the Er sublattice; the short Er–Er doublet which corresponds to two Er(2) of the same subcube is represented by a thick line, the Er(2) tetrahedra by a single line.

Table 4. *Comparison between phase* I *and phase* II *distances* (Å)

Cation–anion distances

Phase I	Average distance	Standard deviation*	Phase II	Average distance	Standard deviation*
Rh–Sn(2)×6	2·649	0	Rh–Sn(3)×4	2·645	0·009
			–Sn(2)×2	2·742	0·005
Yb–Sn(2)×12	3·402	0·004	M(1)–Sn(3)×12	3·393	0·021
Sn(1)–Sn(2)×12	3·309	0	Er(2)–Sn(2)×3	3·212	0·014
			–Sn(3)×6	3·267	0·031
			–Sn(4)×1	3·057	

Cation–cation distances

Phase I	Average distance	Standard deviation*	Phase II	Average distance	Standard deviation*
Rh–Yb×3	3·421	0	Rh–Er(2)×2	3·029	0·021
–M(1)×2	4·190	0	–M(1)×1	3·510	0·011
–Rh×6	4·838	0	–Rh×4	4·741	0·004
			–Rh×4	4·964	0·017
Yb–Rh×4	3·421	0	M(1)–Rh×6	3·510	0·011
–Yb×2	4·838	0	–Er(2)×12	5·651	0·039
–Sn(1)×4	5·409	0			
–Yb×8	5·925	0			
Sn(1)–Rh×8	4·190	0	Er(2)–Er(2)×1	4·376	0
–Yb×12	5·409	0	–Er(2)×3	5·279	0·012
			–Er(2)×2	5·8315	0·020
			–M(1)×3	5·651	0·039

Anion–anion distances and angles in the Rh sites

	Average distance	Standard deviation*	Corresponding Sn–Rh–Sn angle	Standard deviation*
Phase I				
Sn(2)–Sn(2)×6	3·623	0	86·28	0
Sn(2)–Sn(2)×3	3·251	0	75·71	0
Phase II				
Sn(3)–Sn(2)×4	3·659	0·024	85·5	0·6
Sn(3)–Sn(3)×2	3·453	0·008	81·5	0·3
Sn(3)–Sn(3)×2	3·333	0·022	78·1	0·5
Sn(2)–Sn(2)×1	3·415	0·001	77·1	0·1

* These values are the standard deviations calculated from the mean value. If all the distances are the same it is zero.

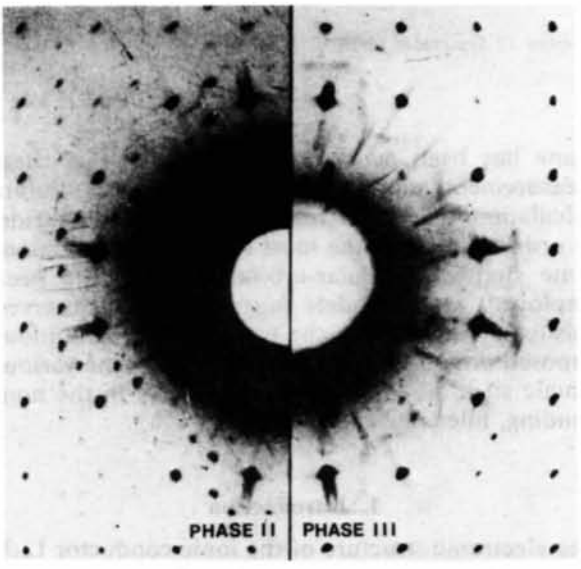

(*a*) (*b*)

Fig. 12. Precession photograph of the two-layer perpendicular to a $[100]_c$ direction of the pseudocubic $2a_{II}\times 2a_{II}\times c_{II}$ cell. (*a*) Phase II. (*b*) Phase III.

Er(2) atoms, causing disorder and twinning, and besides they do not form any short Sn–Sn distances. The M(1), Rh, and Er(2) atoms have a cation-like behavior, while Sn(2) and Sn(3) have an anion-like behavior. The cation–anion distances found in phase II are comparable to the corresponding ones of phase I (Table 4). The Sn(4) atoms participate as anions to the coordination polyhedra of the Er(2) atoms, as Sn(2) and Sn(3), but do not take part in the formation of the Sn-prism framework and have a unique type of bonding. As an anion, Sn(4) is bonded to two Er(2) cations [Sn(4)–Er(2) = 3·057 Å]. However, it is also bonded to two Sn(3) anions [Sn(4)–Sn(3) = 3·138 Å]. This cluster of three Sn atoms seems to be a unique feature and could be compared to the short Sn(2)–Sn(2) bond (2·967 Å) found in phase I and to the short Sn(3)–Sn(3) bond (2·922 Å) in phase II. The small differences among cation–anion, cation–cation, and anion–anion distances indicate that the description in terms of coordination polyhedra built up of cation-like and anion-like atoms is not sufficient. The structure also contains strong metallic bonds among atoms forming isolated clusters. From the description

of the structure as built up of coordination polyhedra, the formula of phase II may be written as: $[Sn(1)_{2/3}Er(1)_{1/3}]^{XII}Er(2)_4^{X}Rh_6^{VI}Sn(2)_4^{VI}Sn(3)_{12}^{V}Sn(4)_2^{II}$. The bonds between anion-like atoms have not been taken into account.

The structures of both phases I and II are built up of $RhSn_6$ trigonal prisms. There is only a small difference between the Sn–Rh distances in the two structures: $6\times2{\cdot}649$; and $4\times2{\cdot}645$ and $2\times2{\cdot}742$ Å, respectively. These distances are far too short to correspond to a metallic character of the bonds. The trigonal prisms are almost undistorted and have comparable Sn–Sn distances and Sn–Rh–Sn angles (see Table 4). The only difference between the two structures is in the prism arrangement and consequently in the rare-earth coordination. It is possible that the trigonal-prism configurations must play an important role in the physical properties of this class of compounds.

References

CHENAVAS, J., HODEAU, J. L., COLLOMB, A., MAREZIO, M., REMEIKA, J. P. & VANDENBERG, J. (1980). Proceedings of the International Conference on Ternary Superconductors, Lake Geneva, Wisconsin, USA.

COOPER, A. S. (1980). *Mater. Res. Bull.* **15**, 799–805.

CROMER, D. T. & LIBERMAN, D. (1970). *J. Chem. Phys.* **53**, 1891–1898.

ESPINOSA, G. P. (1980). *Mater. Res. Bull.* **15**, 791–798.

HODEAU, J. L., CHENAVAS, J., MAREZIO, M. & REMEIKA, J. P. (1980). *Solid State Commun.* **36**, 839–845.

HODEAU, J. L., MAREZIO, M., REMEIKA, J. P. & CHEN, C. H. (1982). *Solid State Commun.* **42**, 97–102.

International Tables for X-ray Crystallography (1974). Vol. IV. Birmingham: Kynoch Press.

LAMBERT, S. E., FISK, Z., HAMAKER, H. C., MAPLE, M. B., WOOLF, L. D., REMEIKA, J. P. & ESPINOSA, G. P. (1980). Proceedings of the International Conference on Ternary Superconductors, Lake Geneva, Wisconsin, USA.

OTT, H. R., ODONI, W., FISK, Z. & REMEIKA, J. P. (1980). Proceedings of the International Conference on Ternary Superconductors, Lake Geneva, Wisconsin, USA.

REMEIKA, J. P., ESPINOSA, G. P., COOPER, A. S., BARZ, H., ROWELL, J. M., MCWHAN, D. B., VANDENBERG, J. M., MONCTON, D. E., FISK, Z., WOOLF, L. D., HAMAKER, H. C., MAPLE, M. B., SHIRANE, G. & THOMLINSON, W. (1980). *Solid State Commun.* **34**, 923–926.

SHENOY, G. K., VICCARO, P. J., CASHION, J. D., NIARCHOS, D., DUNLAP, B. D., PRÖBST, F. & REMEIKA, J. P. (1980). Proceedings of the International Conference on Ternary Superconductors, Lake Geneva, Wisconsin, USA.

VANDENBERG, J. M. (1980). *Mater. Res. Bull.* **15**, 835–847.

Acta Cryst. (1984). B**40**, 38–44

An Investigation of the Electron Density in Li_3N using Compton Scattering. II*

BY PHILIP PATTISON,† NIELS K. HANSEN‡ AND JOCHEN R. SCHNEIDER

Hahn-Meitner-Institut für Kernforschung, Glienicker Strasse 100, *D*-1000 *Berlin* 39, *Federal Republic of Germany*

(*Received* 24 *September* 1982; *accepted* 12 *September* 1983)

Abstract

The results of a series of Compton-profile measurements performed on the superionic conductor Li_3N are reported. The work extends to an earlier study [Pattison & Schneider (1980). *Acta Cryst.* A**36**, 390–398] which supported an ionic model of the electronic distribution in this crystal with an $(Li^+)_3N^{3-}$ configuration. The present results delineate more precisely the evidence for anisotropy in the Compton profile and hence in its Fourier transform. A detailed investigation of the directional dependence of the Fourier-transformed Compton profile within the basal Li_2N plane has been made, and it is hoped that these measurements will provide a useful test for future calculations of the electron density in lithium nitride. In order to identify the most significant interactions some simple molecular-orbital models have been employed. These models suggest that the observed anisotropy arises from the orthogonality conditions imposed on the ionic orbitals centred on the various atomic sites, which produce distortions in the non-bonding, filled shells of electrons.

1. Introduction

The electronic structure of the ionic conductor Li_3N has been for some time a subject of dispute. Theoretical descriptions have ranged from a covalent model as suggested by Krebs (1956, 1968) and Suchet (1961) to an ideal ionic crystal (Schulz & Schwarz, 1978)

* Part I: *Acta Cryst.* (1980). A**36**, 390–398.

† Present address: Fachbereich Chemie, Universität Konstanz, D-7750 Konstanz I, Federal Republic of Germany.

‡ Present address: Laboratoire de Minéralogie et Cristallographie, Université de Nancy I, BP 239, F-54506 Vandoeuvre-Les-Nancy, France.

0108-7681/84/010038-07$01.50